OXFORD

Insula-cingulate structural and functional connectivity: an ultra-high field MRI study

Matthew A. Cormie [ID]¹,², Batu Kaya [ID]¹,², Georgia E. Hadjis [ID]¹,², Pedram Mouseli [ID]¹,², Massieh Moayedi [ID]¹,²,³,⁴,*

¹Centre for Multimodal Sensorimotor and Pain Research, Faculty of Dentistry, University of Toronto, Toronto, ON, Canada,
²University of Toronto Centre for the Study of Pain, Toronto, ON, Canada,
³Krembil Research Institute, University Health Network, Toronto, ON, Canada,
⁴Department of Dentistry, Lunenfeld-Tanenbaum Research Institute, Mount Sinai Hospital, Toronto, ON, Canada

*Corresponding author: Centre for Multimodal Sensorimotor and Pain Research, Faculty of Dentistry, University of Toronto, 501B123 Edward St, Toronto, ON M5G
1E2, Canada. Email: m.moayedi@utoronto.ca

The insula and the cingulate are key brain regions with many heterogenous functions. Both regions are consistently shown to play integral roles in the processing of affective, cognitive, and interoceptive stimuli. The anterior insula (aINS) and the anterior mid-cingulate cortex (aMCC) are two key hubs of the salience network (SN). Beyond the aINS and aMCC, previous 3 Tesla (T) magnetic resonance imaging studies have suggested both structural connectivity (SC) and functional connectivity (FC) between other insular and cingulate subregions. Here, we investigate the SC and FC between insula and cingulate subregions using ultra-high field 7T diffusion tensor imaging (DTI) and resting-state functional magnetic resonance imaging (rs-fMRI). DTI revealed strong SC between posterior INS (pINS) and posterior MCC (pMCC), and rs-fMRI revealed strong FC between the aINS and aMCC that was not supported by SC, indicating the likelihood of a mediating structure. Finally, the insular pole had the strongest SC to all cingulate subregions, with a slight preference for the pMCC, indicative of a potential relay node of the insula. Together these finding shed new light on the understanding of insula-cingulate functioning, both within the SN and other cortical processes, through a lens of its SC and FC.

Key words: pain; MRI; brain; 7T; salience network; diffusion.

Introduction

The insular cortex and anterior and mid-cingulate cortices are large, highly connected brain regions that are commonly activated across brain imaging studies (Hofbauer et al. 2001; Taylor et al. 2009; Kurth et al. 2010; Wiech et al. 2014; Zhao et al. 2022). Both brain regions are unique cortical structures with many heterogenous functions, which has made delineating their precise roles a challenge. The cingulate has functions in motor behavior (Dum et al. 2019) and processing spatial stimuli (Rolls 2019), while the insula has roles in interoceptive awareness (Craig 2003, 2009) and gustatory regulation (Stephani et al. 2011). There are five primary subregions of the cingulate cortex: the subgenual anterior-cingulate cortex (sgACC), rostral anterior-cingulate cortex (rACC), anterior mid-cingulate cortex (aMCC), posterior mid-cingulate cortex (pMCC), and the posterior cingulate cortex (PCC) (Vogt 2005). There are four primary subregions of the insula: posterior insula (pINS), mid insula (mINS), anterior insula (aINS), and the insular pole (poINS) (Stephani et al. 2011; Cloutman et al. 2012). One intrinsic brain network comprising regions from both the insula and cingulate is the salience network (SN), which responds to attention-grabbing—i.e. salient—stimuli and guides behavior in response to those stimuli (Seeley et al. 2007). The SN has also been hypothesized to act as a hub that shifts attentional resources to external stimuli, specifically acting as a mediator between the default mode network (DMN) and central executive network (CEN) (Sridharan et al. 2008; Menon and Uddin 2010; Manuello et al. 2018; Varjacic et al. 2018; Li et al. 2022). In addition to the insula and cingulate, the SN comprises subcortical regions including the amygdala, substantia nigra, ventral tegmental area, and the thalamus (Seeley et al. 2007). The primary connections of the SN, however, are between its two key nodes: the insula and the cingulate cortex (Sridharan et al. 2008; Menon and Uddin 2010; Uddin 2015).

Neuroimaging studies investigating the functional connectivity (FC) between the insula and cingulate in the SN have consistently focused on the aINS and the aMCC (Peyron et al. 2000; Craig 2002; Eisenberger et al. 2003; Singer et al. 2004; Singer 2006; Immordino-Yang et al. 2009; Zaki et al. 2016). These two brain regions are involved in the processing of stimuli with affective and motivational components, including nociceptive and empathetic pain processing (Singer et al. 2004; Zaki et al. 2016), complex emotional states (Immordino-Yang et al. 2009), social rejection (Eisenberger et al. 2003), pleasurable touch, hunger, and metabolic stress (Craig 2002).

Another key region of the insula, the pINS, has been shown to be consistently involved in sensory and interoceptive processing (Craig 2003), and receives information such as thirst, hunger, pain, temperature, and itch (Augustine 1996; Ostrowsky et al. 2002; Craig 2003; Brooks et al. 2005; Stephani et al. 2011; Lerman et al. 2019). Notably, nonhuman primate tract tracing studies and some human neuroimaging studies at 1.5 Tesla (1.5 T) and 3 Tesla (3T) have not identified dense structural connectivity (SC) between the pINS and the pMCC (Mufson and Mesulam 1982; Mesulam and Mufson 1982a, 1982b; Craig 2002, 2003; Taylor et al. 2009; Wiech et al. 2014; Ghaziri et al. 2015). Although some imaging studies at 3T have observed both a SC and FC between the pINS and

the pMCC (Taylor et al. 2009; Wiech et al. 2014), ultra-high field diffusion-weighted imaging (DWI) scans are better able to discern discreet white matter tracts given the increased signal-to-noise ratio in comparison to the more common 3T scanner (Dyvorne et al. 2016), with better resolution of crossing fibers (Behrens et al. 2007; Mukherjee et al. 2008; Descoteaux et al. 2009).

Here, we used ultra-high field DWI scans from the Human Connectome Project (HCP) (Van Essen et al. 2013) to identify the SC between subregions of the insula and cingulate. Additionally, we investigated the resting state FC between four key insula subregions and three key cingulate subregions to determine whether there was correspondence between SC and FC. Finally, to complement predefined insular and cingulate subregions, we performed a SC-based parcellation to identify subregions of the insula and cingulate based on their SC profiles to subregions of the insula or cingulate.

Materials and methods
Participants

All data used in this study were acquired from participants in the Washington University and University of Minnesota (WU-Minn) HCP S1200 Release (Van Essen et al. 2013). The WU-Minn S1200 release is the most recent release involving healthy young adult neuroimaging to date, and therefore has the most vigorous quality control of any other HCP cohort of young adults and their neuroimaging data (S1200 website: https://www.humanconnectome.org/study/hcp-young-adult/document/1200-subjects-data-release).

Inclusion and exclusion criteria for the HCP WU-Minn S1200 cohort are provided elsewhere (Van Essen et al. 2012). Briefly, participants were between the ages of 22 and 36+ years, with no history of neurological, psychological, or cardiovascular disorders, obtained a score ≥ 29 on the Mini Mental State Exam (Kurlowicz and Wallace 1999), and provided informed consent. Exclusion criteria included any genetic disorders, ≥ 2 unprovoked seizures, or an epilepsy diagnosis, cerebral palsy, multiple sclerosis, stroke, brain tumor, sickle cell disease, history of head trauma, premature birth, pregnancy, current chemotherapy, or immunomodulatory agents, thyroid treatment in the last 12 months, diabetes treatment in the last 12 months, use of migraine medication in the last 12 months, and MRI contraindications.

All analyses herein were approved by the University of Toronto Human Research Ethics Board.

175 participants with 3T structural, 7T DWI and resting-state functional magnetic resonance imaging (rs-fMRI) scans (68 males, 107 females; mean age ± SD: 29.6 ± 3.1 years) from HCP's S1200 young adult database were included in this study (Van Essen et al. 2013). All 184 participants within the HCP's S1200 young adult database with 7T data were screened, and 9 were excluded due to missing rs-fMRI data or corrupted files.

HCP neuroimaging parameters

All participants underwent imaging in both 7T and 3T MRI scanners. 3T scans were acquired using a customized 3T Siemens "Connectome Skyra," which used a standard 32-channel head coil and a body transmission coil. The 7T scans were acquired with a Siemens Magnetom scanner at the University of Minnesota's Center for Magnetic Resonance, using a Nova32 32-channel Siemens receive head coil with a head-only transmit coil incorporated that surrounds the receive coil from Nova Medical.

Whole brain structural T1- and T2-weighted scans were acquired only at 3T. The T1 scans were acquired using the

following parameters: echo time (TE) = 2.14 ms, repetition time (TR) = 2,400 ms, inversion time (TI) = 1,000 ms, voxel size = 0.70 mm isometric, field of view (FOV) = 224 × 224 (Van Essen et al. 2012).

The 7T DWI scans were obtained over four runs with the following parameters: spin-echo echo-planar imaging (EPI), 132 slices, 1.05 mm isotropic voxels, TR = 7,000 ms, TE = 71.2 ms, FOV = 210 × 210. Each of the scans were acquired from two sets of gradients, each with a different b-value. Each set contained 65 diffusion-weighted directions and six nondiffusion weighting images (B0) distributed across each run. Diffusion weighting consisted of two shells (b = 1,000 and 2,000 s/mm^2), interspersed with an equal number of acquisitions of each shell within each run (Moeller et al. 2010; Feinberg et al. 2011; Setsompop et al. 2012; Xu et al. 2012). The Emmanuel Caruyer toolbox was used to help ensure uniform distribution of directions across multiple q-space shells (Caruyer et al. 2013). Acquisitions were performed with once posterior-to-anterior and once anterior-to-posterior encoding polarities (Van Essen et al. 2012).

The 7T rs-fMRI scans were obtained over four runs with the following parameters: gradient-echo EPI, 1.6 mm isotropic voxels, TR = 1000 ms, TE = 22.2 ms, FOV = 208 × 208 (Moeller et al. 2010; Feinberg et al. 2011; Setsompop et al. 2012; Xu et al. 2012). Acquisitions were performed with twice posterior-to-anterior and once anterior-to-posterior encoding polarities (Van Essen et al. 2012).

MRI and statistical analysis
HCP preprocessing

Preprocessed DWI and rs-fMRI data were downloaded from the HCP (Jenkinson et al. 2002; Glasser et al. 2013).

The HCP preprocessing pipelines utilize tools from the FreeSurfer image analysis suite [v.5.3.0-HCP; (Dale et al. 1999)]. T1-weighted scans underwent the HCP PreFreeSurfer pipeline (v3). This pipeline corrects for gradient distortions then rigidly aligns the T1 scans (6 degrees of freedom) to the MNI152 template using FSL's linear registration algorithm (FLIRT) (Jenkinson and Smith 2001; Jenkinson et al. 2002).

The generic HCP MR diffusion preprocessing pipeline (v3.19.0) includes intensity normalization across runs and EPI distortion correction using FSL's TOPUP and EDDY (v.5.0.10) to account for motion artifacts and eddy currents (Andersson et al. 2003; Andersson and Sotiropoulos 2015). Scanner gradient nonlinearities were then corrected by spatially warping the images using scanner specific information (Jovicich et al. 2006). Finally, mean B0 images were registered, using FLIRT, to native volume T1 images.

The generic HCP MR resting-state preprocessing pipeline (v3.21.0) includes gradient distortion correction, FLIRT-based motion correction, TOPUP-based field map preprocessing, EPI to T1w registration, spline resampling, and intensity normalization to a mean of 10,000 (Glasser et al. 2013). Resting-state data also underwent independent component analysis (ICA)- FMRIB's ICA-based X-noisifier (FIX) denoising (Glasser et al. 2013; Griffanti et al. 2014; Salimi-Khorshidi et al. 2014).

Study specific preprocessing

A summary of the preprocessing steps is provided in Supplementary Fig. S2. Every participant's DWI scan underwent track estimation using FSL's Bayesian Estimation of Diffusion Parameters Obtained using Sampling Techniques-Crossing Fibers [BEDPOSTx; (Behrens et al. 2003; Behrens et al. 2007)] tool. BEDPOSTx was run to estimate fiber orientation of each voxel in the brain, using a two-fiber model. BEDPOSTx runs a model where the diffusion coefficient is modeled using a Gamma distribution (Jbabdi et al. 2012).
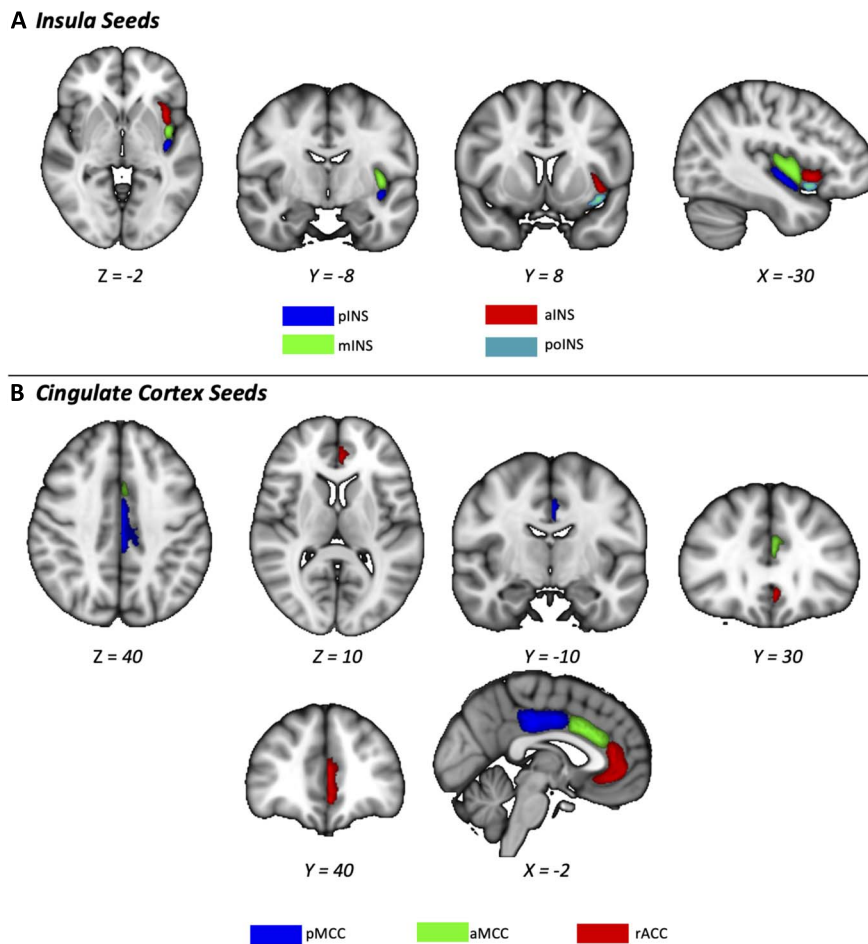
Fig. 1. Insula and cingulate subregion masks. Group mask of insula subregions is shown (**A**) with the subregions: pINS in dark blue, mINS in green, aINS in red, and poINS in light blue. Group mask of cingulate cortex subregions is shown (**B**) with the subregions: pMCC in blue, aMCC in green, and rACC in red. All subregion masks were at a 50% threshold overlap between all participants.

As participants' rs-fMRI scans were already preprocessed prior to downloading, the only additional step to run was spatial filtering with a 5 mm full-width at half-maximum (FWHM) Gaussian kernel.

Region of interest definition
Insula

Parcellation schemes comprising insular subregions were not available in the parcellations schemes provided with FreeSurfer. Therefore, subregions were manually delineated in individual participant space. Previous literature has functionally segregated the insula into (i) posterior subregion caudal to the postcentral sulcus of the insula, (ii) a mid-insula subregion between the postcentral sulcus and the precentral sulcus of the insula, and (iii) an anterior subregion rostral to the precentral sulcus of the insula (Stephani et al. 2011). For this study, the insula was parcellated, bilaterally, into four subregions: pINS, mINS, aINS, and poINS. The posterior subregions comprised the posterior long gyrus (caudal to the postcentral sulcus); the mid subregions comprised the anterior long gyrus and the posterior short gyrus (between the postcentral and precentral sulcus); the anterior subregions comprised the mid and anterior short gyrus (cranial from the precentral sulcus) (Stephani et al. 2011); and the poINS subregion comprised the transverse gyrus and limen (Türe et al. 1999) (Fig. 1A).

A probabilistic atlas of the four insula subregions, from 48 participants, was manually delineated by MAC. All insula subregion masks were visually compared to ensure standardization of subregion segmentation across participants. Subregions were then converted to MNI152 template space, binarized, and combined to form a probabilistic mask of the insula (see Supplement). This probabilistic atlas was thresholded at 25%, then nonlinearly registered to the remaining 127 participants' native space, using FSL's FNIRT (Jenkinson et al. 2012). All subregions were then visually inspected to ensure correct registration and standardization of segmentation.

Cingulate cortex

Cingulate subregions were extracted from the Desikan-Killiany Atlas (Desikan et al. 2006) implemented in FreeSurfer [v.5.3.0-HCP; (Dale et al. 1999)]. The atlas comprised four subregions for the cingulate cortex, of which three were used in this study: the rACC, the caudal aMCC, and the pMCC (Vogt et al. 2003; Vogt 2016) (Fig. 1B).

Probabilistic tractography
Insula-cingulate subregion SC

Probabilistic tractography was performed in FSL's Probtrackx (Behrens et al. 2003; Behrens et al. 2007) to assess direct insula-cingulate SC. In total, 48 tractograms were constructed in participants' native space—24 for each hemisphere. Within the same hemisphere, two tractograms with opposing directions (i.e. A-to-B and B-to-A) were constructed for each circuit to account

for directional biases from acquisition (Van Essen et al. 2014) and fiber fanning as a feature of tracking direction (Jeurissen et al. 2019). When generating tractograms, the modified Euler algorithm was used, with 10,000 streamlines per voxel. To reduce the likelihood of spurious connections, and unrelated tracts being delineated, we included an exclusion mask (Supplementary Fig. S1) that comprised the following to limit and guide tractography:

(i) a midsagittal exclusion mask to remove tracts crossing the midline into the other hemisphere;
(ii) an anterior coronal exclusion mask was added to remove prefrontal radiating tracts leading away from the cingulate. The mask was drawn as a coronal section anterior to the rACC;
(iii) a posterior coronal exclusion mask to remove posterior radiating tracts from the insula;
(iv) a partial exclusion mask of the corpus collosum to exclude crossing fibers, but still retained much of the bundle to ensure potential tracts directly adjacent to the cingulate cortex was not excluded;
(v) a thalamus exclusion mask to avoid network connections between these regions and the thalamus (Seeley et al. 2007);
(vi) similarly, an amygdala mask to reduce network connections between these regions and the amygdala (Seeley et al. 2007);
(vii) to control for the direction of streamline propagation, we configured each tractography analysis to propagate toward and not past the insula for tracts originating from the cingulate, or the cingulate as a terminal point for tracts originating from the insula.

During analysis, bidirectional tractograms were corrected for seed region-of-interest (ROI) size, averaged and thresholded (See *Quantifying probabilistic tractography outputs*) to generate a final tractogram per circuit, per hemisphere—for a total of 24 for the whole brain: right and left pINS-rACC, pINS-aMCC, pINS-pMCC; mINS-rACC, mINS-aMCC, mINS-pMCC; aINS-rACC, aINS-aMCC, aINS-pMCC; poINS-rACC, poINS-aMCC, and poINS-pMCC.

Seed-to-voxel connectivity and find_the_biggest

To mitigate the limitations of predefining seed regions, a connectivity-based seed classification using FSL's probabilistic tractography (Behrens et al. 2003; Johansen-Berg et al. 2004) was run from each subregion to the whole of the other structure. For example, aMCC to whole insula, or aINS to whole cingulate. A total of 24 analyses were run in each participant's native space, 12 in each hemisphere, and one for each ROI. A modified Euler algorithm, with 10,000 streamlines per voxel was used. Identical exclusion masks were applied as those used in the ROI-to-ROI analyses (Supplemental Fig. S1). Each tractogram was corrected for seed size, averaged and thresholded to generate final tractograms. FSL's *find_the_biggest* tool was used to classify seed voxels according to the target mask with the highest probability of connection, outputting a final parcellated mask of the insula or cingulate (Behrens et al. 2003; Johansen-Berg et al. 2004).

Connectivity-based parcellation group mask

To visualize trends in the average seed-to-voxel connectivity (mentioned in *Seed-to-Voxel Connectivity and find_the_biggest*), group masks were created by converting all final tractograms from participants' native space to MNI152 template space (Jenkinson and Smith 2001; Jenkinson et al. 2002). Participant masks were then binarized, summed, and thresholded at 25%, to make a final probabilistic group mask.

rs-fMRI analysis

All ROIs were converted from individual participant space to MNI152, then from FSL MNI152 space to participant's functional space, using FLIRT (Jenkinson et al. 2012). Next, the average time-series for each ROI in functional space were extracted. To quantify resting-state FC between insula and cingulate subregions, ROI-to-ROI connectivity was calculated by correlating timeseries between regions (e.g. correlating timeseries between left aMCC and left aINS) using Spearman's Rank Correlation. The distribution of timeseries activity was not normally distributed, and as such nonparametric testing was used in analysis. Each insula-cingulate correlation then underwent Fisher Z-Transformation to standardize individual correlations across all participants and calculate median correlation before transforming back to undergo Spearman's Rank Correlation to determine group average correlations.

Statistical analyses
Quantifying SC from probabilistic tractography outputs

The SC strength was calculated from the waytotal count, which is the number of fibers sent from the initial ROI that arrived at the target ROI. Given that we set Probtrackx to send 10,000 streamlines from each voxel of the seed, the number of total streamlines is equivalent to 10,000 multiplied by the number of voxels in the seed mask. To normalize the number of streamlines, due to the uneven number of voxels in each seed, we divided the waytotal count by the number of voxels in the initial seed region mask. The normalized tracts from the same pathway (e.g. right pINS to rACC, right rACC to pINS) were then averaged to control for directionality. This final value for each tractogram is termed the connectivity strength and is an arbitrary unit (a.u.). These steps were repeated for every pair of tracts resulting in 24 connectivity strength metrics (i.e. waytotal counts) for each participant (these are the same circuits as listed in the *Probabilistic tractography* section). Nonparametric tests by ranks were employed (see below), which are robust to potential outliers (Hettmansperger 2011), and, as such, no individual connectivities were excluded from connectivity strength analyses.

All statistical tests were performed in SPSS Statistics v 28.0.1.1 for Mac (IBM SPSS Statistics, Armonk, NY, USA). Normality was first tested using the Kolomogrov-Smirnov test, which is robust for sample sizes with > 50 participants (Mishra et al. 2019). We found a non-normal distribution ($P < 0.05$), and thus nonparametric tests were used. Related-Samples Friedman's Two-Way Analysis of Variance by Ranks was performed to determine the connectivity strengths between each insula subregion and each cingulate subregion. Significance was set at $\alpha < 0.05$. Wilcoxon signed-ranks test was then used to determine significant differences in SC between insula and each cingulate subregions, and vice-versa, with significance set at $P < 0.05$. The SC of each hemisphere was first analyzed independently, then each insula-cingulate connectivity was analyzed across hemisphere as well (e.g. left hemisphere aINS-aMCC vs right hemisphere aINS-aMCC).

Quantifying FC outputs

Once group average correlations were calculated for each insula-cingulate connectivity, significance could be calculated using Bonferroni correction for 12 independent samples. The Bonferroni corrected significance threshold was set to $P < 0.004$, meaning a ρ of 0.215 is required to achieve significance, based on the sample size. To measure if age influences FC, Fisher Z-transformation was run, and a Spearman correlation was used to determine

any significant differences in FC for each insula-cingulate connection based on age. For sex, a similar method was employed using a Fisher Z-transformation, then calculating the median FC. The male and female FC strengths for each insula-cingulate subregion were compared using a Wilcoxon-signed ranks test to identify any significant differences. Significance was then corrected for multiple comparisons using the false discovery rate, with $q < 0.05$.

Results
Insula-cingulate ROI-to-ROI SC
Normality testing
Connectivity strengths between every insula subregion with the three cingulate subregions for each hemisphere were tested for normality using a Kolmogorov–Smirnov test. Within both the right and left hemisphere, at least one insula-cingulate circuit was not normally distributed ($P < 0.05$).

Left hemisphere
Within the left hemisphere, the Friedman's Two-way Analysis identified significant differences between insula-cingulate connectivities ($\chi^2(11) = 1208, P < 0.001$).

Comparing the median SC strengths (a.u.) between each insula-cingulate connection (Fig. 2A), it is apparent the poINS has overall the strongest connections to each cingulate subregion, with the strongest connection to the pMCC. Further, of the cingulate subregions, the pMCC tends to have the strongest connections to insula subregions, followed by the aMCC then rACC. Overall, the mINS has the lowest median connectivity to each cingulate subregion. Excluding the poINS, the pINS and aINS have a relatively strong median connection to the pMCC.

Further analysis directly comparing SC strengths of insula subregion to each cingulate subregion was conducted using a Wilcoxon signed-rank test (Table 1, Fig. 2B). All insula subregions have the strongest connections to the pMCC, followed by the aMCC, then rACC ($P < 001$; Fig. 2B), excluding the poINS. The poINS does show a significantly stronger connection to the pMCC vs aMCC ($P < 0.01$; Fig. 2B) and stronger connection to the pMCC vs rACC ($P = 0.002$), but no significant difference in its connection to the aMCC vs rACC ($P = 0.061$).

When comparing cingulate subregions, Wilcoxon signed-ranks reveals that only the rACC has significantly different SC to every insula subregion (Table 1, Fig. 2C). The aMCC has the strongest SC to the poINS ($P < 0.001$; Fig. 2C), followed by the aINS ($P < 0.001$), then the pINS and mINS ($P = 0.758$), but the difference in connectivity strength between these two connections (aMCC-pINS vs aMCC-mINS) was not significantly different. The pMCC has the strongest connections to the poINS ($P < 0.001$; Fig. 2C), followed by the pINS and aINS, which are not significantly different ($P = 0.309$), then finally the mINS ($P < 0.001$). The rACC has the same strongest connection to the poINS, followed by the aINS, pINS then mINS, all of which are significantly different ($P < 0.001$; Fig. 2C).

Right hemisphere
Within the right hemisphere, the Friedman's Two-way Analysis identified significant differences between insula-cingulate connectivities ($\chi^2(11) = 1061, P < 0.001$).

Similar to the left hemisphere, comparing the median SC strengths (a.u.) between each insula-cingulate connection in the right hemisphere (Fig. 2A) shows a similar pattern, with the poINS having the overall the strongest connections to each cingulate subregion, and the strongest connection to the pMCC. The pMCC tends to have the strongest connections to insula subregions, followed by the aMCC then rACC, with the aMCC and rACC showing similarly weak SC strengths. The mINS and aINS appear to have the lowest median connectivity to each cingulate subregion, except to the aMCC, where the mINS has a marginally stronger connection. Following the poINS, the pINS has a relatively strong median connection to the pMCC.

Comparing SC strengths of insula subregion to each cingulate subregion using a Wilcoxon signed-rank test (Table 2, Fig. 2D), shows that every insula subregion has a statistically significant difference in its SC to each cingulate subregion. The pINS, mINS, and aINS all show a strong preferential connection to first the pMCC, then the aMCC, followed by the rACC ($P < 0.001$; Fig. 2D). The poINS shows the same patterns with a less drastic difference in connection to the aMCC vs rACC (effect size = 0.247; $P = 0.005$; Fig. 2D).

Comparing cingulate subregions, Wilcoxon signed-ranks reveals the same preferential connection to the poINS, except in the pMCC (Table 2, Fig. 2E). The aMCC shows the strongest connection to the poINS ($P < 0.001$; Fig. 2E), followed by the mINS, then pINS, and aINS, with only the connection to the mINS vs aINS being significantly different ($P = 0.024$). In the case of the pMCC, the strongest connection is to both the pINS and poINS, with no significant difference in SC between the two ($P = 0.892$; Fig. 2E). The pMCC's connection to the aINS and mINS is significantly different compared to the pINS and poINS ($P < 0.001$; Fig. 2E), but not significantly different between each other ($P = 0.244$). The rACC shows the strongest SC to the poINS ($P < 0.001$; Fig. 2E), followed by the pINS ($P < 0.001$), the aINS, and the mINS ($P = 0.017$).

Bilateral analysis
Comparing both the right and left hemispheres, Friedman's Two-way Analysis identified significant differences between insula-cingulate connectivities ($\chi^2(23) = 2,128, P < 0.001$).

Wilcoxon signed-rank test was used to directly compare insula-cingulate connections between the left and right hemispheres, to determine any significant differences in hemispheric SC (Table 3). In comparing the mINS connection to each cingulate subregion, the left and right hemispheres do not have any significant difference in their SC ($P > 0.05$; Table 3). The pINS shows a stronger SC to the pMCC in the right vs left hemisphere ($P = 0.004$; Table 3), but no significant difference between hemispheres in its connection to the aMCC or rACC ($P > 0.05$). The left aINS shows a stronger SC to every cingulate subregion compared to the right hemisphere ($P < 0.005$; Table 3). The poINS shows a similar pattern, with the strongest SC to all cingulate regions in the left vs right hemisphere ($P < 0.001$; Table 3).

7T vs 3T SC analysis
In a subset of 48 participants, SC was compared using 3T and 7T scans to determine any key differences in the two image resolutions (Supplementary Fig. S3). Overall, both the 3T and 7T scans show a similar pattern of connectivity. Notably, they both show a strong SC between the poINS to all cingulate subregions, with the strongest to the pMCC. Additionally, they both show a strong aINS connection to the pMCC, and a relatively strong connection to the aMCC. However, the 3T scans appear to show an overall higher connectivity strength (a.u.) compared to the 7T scans. A key difference between the two scans is the 3T
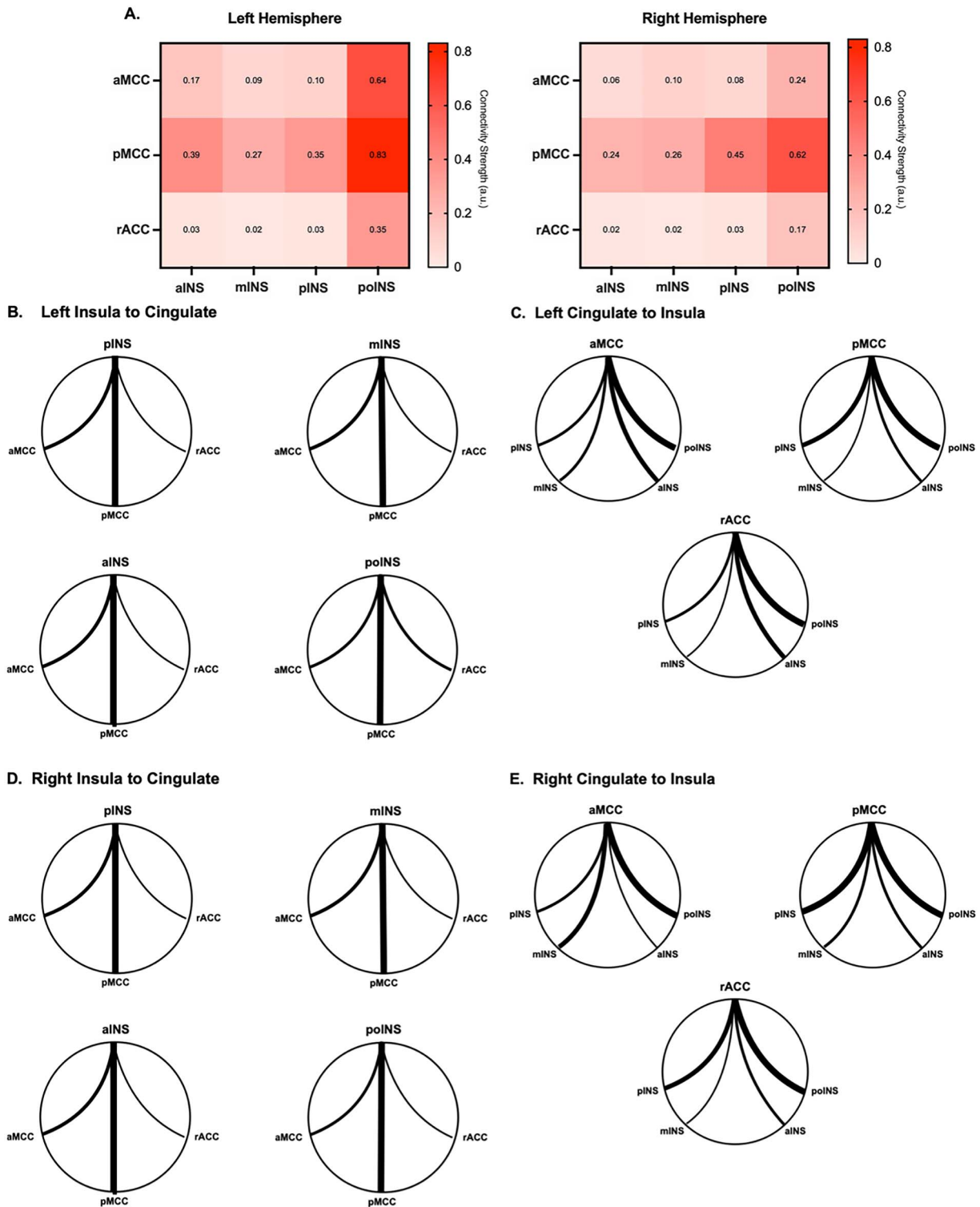
Fig. 2. SC strengths between insula-cingulate subregions. Left and right hemisphere connectivity correlation matrix (**A**) between insula and cingulate subregions. Functional connectome maps of left insula to cingulate subregions (**B**), left cingulate to insula subregions (**C**), right insula to cingulate subregions (**D**), and right cingulate to insula subregions (**E**). Connectome maps created from connectivity strength ranking from Wilcoxon-signed ranks analysis. Line thickness represents a stronger relative connectivity compared to other regions. Variation in thickness represents significant differences in connectivity, while identical thickness indicates no significant differences.

scans show a stronger relative SC between the left poINS and aMCC, while the 7T scans show a stronger relative SC between the right pINS and pMCC. Each scan was taken on different scanners, therefore direct comparisons cannot be reliably concluded.

Insula-cingulate SC-based parcellation
Left insula

SC-based parcellation of the left insula is present in Fig. 3. Parcellation of the insula from pMCC connections indicates a strong SC to primarily the aINS and rostral poINS. It also has some

Table 1. Pairwise comparison of connectivity strength of insula and cingulate subregions in the left hemisphere. Wilcoxon signed-rank test comparing the connectivity strength (a.u.) of insula subregions to each cingulate subregion, and cingulate to each insula subregion.

			Statistic (W)	P	Effect size
Insula to Cingulate					
	pINS	aMCC vs pMCC	1,200	<0.001	−0.844
		aMCC vs rACC	14,004	<0.001	0.819
		pMCC vs rACC	15,259	<0.001	0.982
	mINS	aMCC vs pMCC	1,590	<0.001	−0.794
		aMCC vs rACC	14,212	<0.001	0.846
		pMCC vs rACC	15,063	<0.001	0.956
	aINS	aMCC vs pMCC	2,091	<0.001	−0.728
		aMCC vs rACC	13,941	<0.001	0.811
		pMCC vs rACC	14,964	<0.001	0.943
	poINS	aMCC vs pMCC	5,450	<0.001	−0.292
		aMCC vs rACC	8,957	0.061	0.163
		pMCC vs rACC	9,748	0.002	0.266
Cingulate to Insula					
	aMCC	pINS vs mINS	7,907	0.758	0.0269
		pINS vs aINS	3,906	<0.001	−0.4927
		pINS vs poINS	785	<0.001	−0.8981
		mINS vs aINS	3,204	<0.001	−0.5839
		mINS vs poINS	804	<0.001	−0.8956
		aINS vs poINS	816	<0.001	−0.894
	pMCC	pINS vs mINS	10,641	<0.001	0.3819
		pINS vs aINS	7,017	0.309	−0.0887
		pINS vs poINS	3,267	<0.001	−0.5757
		mINS vs aINS	3,933	<0.001	−0.4892
		mINS vs poINS	1,254	<0.001	−0.8371
		aINS vs poINS	1,614	<0.001	−0.7904
	rACC	pINS vs mINS	10,163	<0.001	0.3199
		pINS vs aINS	5,363	<0.001	−0.3035
		pINS vs poINS	407	<0.001	−0.9471
		mINS vs aINS	3,236	<0.001	−0.5797
		mINS vs poINS	74	<0.001	−0.9904
		aINS vs poINS	67	<0.001	−0.9913

Effect size was calculated using rank biserial correlation (Kerby 2014). Abbreviations: pINS, posterior insula; mINS, mid insula; aINS, anterior insula; poINS, insular pole; aMCC, anterior mid-cingulate cortex; pMCC, posterior mid-cingulate cortex; rACC, rostral anterior-cingulate cortex.

weaker connections to the dorsal region of mINS for the pINS. Parcellation from the aMCC clusters around the aINS and poINS, with some spurious connections to the dorsal mINS. rACC to insula parcellation indicates a strong preferential connection to the poINS. Overall, the pMCC has the most voxels indicating the strongest primary SC to most of the insula, followed by the aMCC then rACC. The pMCC is the only cingulate region that appears to have strong preferential connections to the posterior regions of the insula.

Right insula

SC-based parcellation of the right insula is present in Fig. 3. Parcellation of the insula from the pMCC indicates a preferential SC to the dorsal pINS, mINS, and aINS, as well as the rostral poINS. Parcellation from the aMCC is clustered primarily around the aINS, and rostral poINS, with some spurious connections through the dorsal mINS. Parcellation from the rACC is isolated to the poINS. Both the pMCC and aMCC have similar voxel counts, indicating both have similar primary SC to the insula, followed by the rACC. SC-parcellation shows an isolation of the aMCC to primarily the anterior regions of the insula, while the pMCC has connection to both posterior and anterior regions.

Left cingulate cortex

SC-based parcellation of the left cingulate cortex is present in Fig. 4. Parcellation of the cingulate cortex from the pINS indicates

strong SC to the pMCC and aMCC, with preference for the posterior regions of the cingulate. The pINS also shows some spurious connections into the rACC. Parcellation from the mINS indicates a preferential SC to the pMCC, with weaker connections into the aMCC. Parcellation from the poINS has strong connection to all cingulate subregions, and is the insula region with primary connections to the rACC. Parcellation from the aINS appears to be relatively equally connected to the pMCC and aMCC, with the primary focus of the connections on the border of the two regions. It also shows some spurious connections into the rACC. Overall, the poINS shows the strongest connections based on voxel count, followed by the pINS, then the aINS and mINS, which are relatively similar.

Right cingulate cortex

SC-based parcellation of the right cingulate cortex is present in Fig. 5. Parcellation of the cingulate cortex from the pINS shows a strong preference for posterior regions of the cingulate, more specifically the pMCC, with some spurious connections into the aMCC. Parcellation from the mINS shows a similar preferential SC to the pMCC, with weaker connection to the posterior region of the aMCC. Parcellation from the poINS shows strong SC to all cingulate subregions, making it the only insula subregion showing strong SC into the rACC. Parcellation from the aINS shows preferential connection to the aMCC, some to the pMCC, and very weak connection to the rACC.

Table 2. Pairwise comparison of connectivity strength of insula and cingulate subregions in the right hemisphere. Wilcoxon signed-rank test comparing the connectivity strength (a.u.) of insula subregions to each cingulate subregion, and cingulate to each insula subregion.

		Statistic (W)	P	Effect size
Insula to Cingulate				
pINS	aMCC vs pMCC	331	<0.001	−0.957
	aMCC vs rACC	13,931	<0.001	0.851
	pMCC vs rACC	15,263	<0.001	0.982
mINS	aMCC vs pMCC	2,217	<0.001	−0.709
	aMCC vs rACC	14,906	<0.001	0.936
	pMCC vs rACC	15,231	<0.001	0.978
aINS	aMCC vs pMCC	1,692	<0.001	−0.78
	aMCC vs rACC	13,908	<0.001	0.827
	pMCC vs rACC	15,004	<0.001	0.949
poINS	aMCC vs pMCC	3,309	<0.001	−0.57
	aMCC vs rACC	9,490	0.005	0.247
	pMCC vs rACC	11,304	<0.001	0.468
Cingulate to Insula				
aMCC	pINS vs mINS	7,224	0.479	−0.0618
	pINS vs aINS	8,683	0.108	0.1406
	pINS vs poINS	2,737	<0.001	−0.6405
	mINS vs aINS	9,219	0.024	0.1973
	mINS vs poINS	2,439	<0.001	−0.6832
	aINS vs poINS	1,078	<0.001	−0.8584
pMCC	pINS vs mINS	11,850	<0.001	0.539
	pINS vs aINS	11,404	<0.001	0.481
	pINS vs poINS	7,792	0.892	0.0119
	mINS vs aINS	8,483	0.244	0.1017
	mINS vs poINS	2,502	<0.001	−0.6751
	aINS vs poINS	1,645	<0.001	−0.7864
rACC	pINS vs mINS	11,803	<0.001	0.5505
	pINS vs aINS	10,774	<0.001	0.4153
	pINS vs poINS	1,771	<0.001	−0.7674
	mINS vs aINS	6,027	0.017	−0.2083
	mINS vs poINS	148	<0.001	−0.9806
	aINS vs poINS	403	<0.001	−0.9471

Effect size calculated using rank biserial correlation (Kerby 2014). Abbreviations: pINS, posterior insula; mINS, mid insula; aINS, anterior insula; poINS, insular pole; aMCC, anterior mid-cingulate cortex; pMCC, posterior mid-cingulate cortex; rACC, rostral anterior-cingulate cortex.

Table 3. Insula-cingulate connectivity strength comparison between hemispheres: Wilcoxon signed-rank test comparing the connectivity strength (a.u) of insula-cingulate connectivities in the left vs right hemisphere.

		Statistic (W)	P	Effect size
pINS to aMCC	Left vs Right	7,038	0.324	−0.0860
pINS to pMCC		5,740	0.004	−0.2545
pINS to rACC		7,154	0.416	−0.0709
mINS to aMCC		6,691	0.133	−0.1310
mINS to pMCC		6,777	0.169	−0.1199
mINS to rACC		8,846	0.088	0.1488
aINS to aMCC		10,781	<0.001	0.4001
aINS to pMCC		9,617	0.004	0.2490
aINS to rACC		10,898	<0.001	0.4153
poINS to aMCC		10,668	<0.001	0.3855
poINS to pMCC		10,101	<0.001	0.3118
poINS to rACC		10,732	<0.001	0.3938

Effect size calculated using rank biserial correlation (Kerby 2014). Abbreviations: pINS, posterior insula; mINS, mid insula; aINS, anterior insula; poINS, insular pole; aMCC, anterior mid-cingulate cortex; pMCC, posterior mid-cingulate cortex; rACC, rostral anterior-cingulate cortex.

Insula-cingulate ROI-to-ROI FC

All FC analyses were conducted within their respective hemispheres. Analyses were run on an ROI-to-ROI basis determining the relative correlation in activity between each insula and cingulate subregion.

Left hemisphere

Left hemisphere FC between each insula-cingulate connectivity is presented in Fig. 6. The effect of age on FC was tested, finding significant differences in the poINS-pMCC ($\rho = 0.0019$; $P = 0.0229$) and poINS-rACC ($\rho = 0.0033$; $P = 0.0359$) connectivities. The effect of
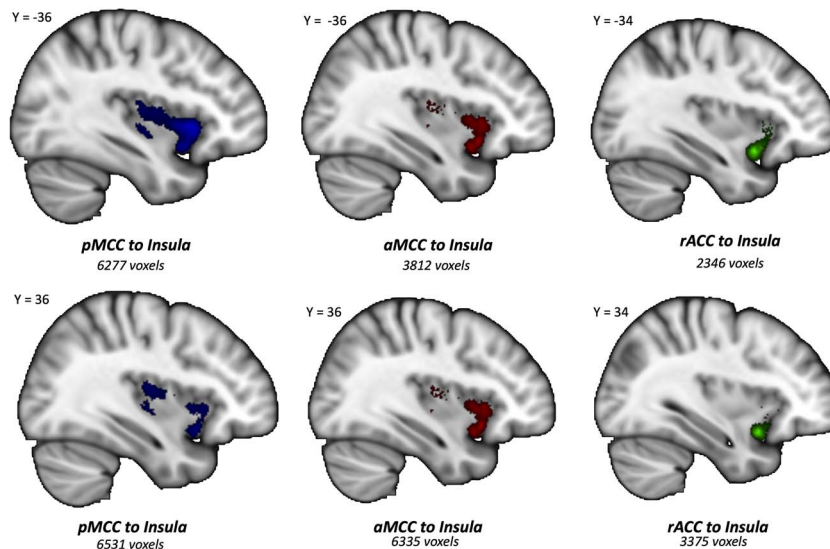
Fig. 3. Insula connectivity based parcellation: group mask of insula parcellation based on maximum probability of connection to cingulate subregions for left insula (upper panel) and right insula (lower panel). Probabilistic masks thresholded at 25%. Total voxel count of each parcellation included for each subregion.
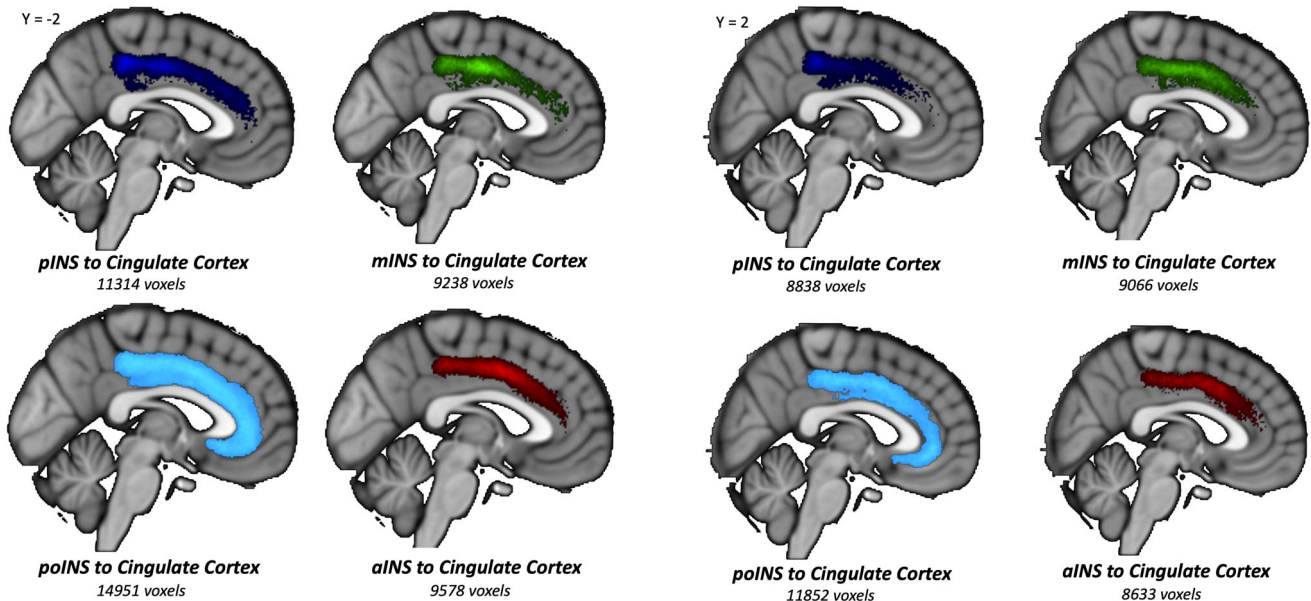

Fig. 4. Left cingulate SC-based parcellation. Group mask of cingulate cortex parcellation based on maximum connectivity probability to insula subregions. Masks thresholded at 25% after creation of mask. Total voxel count of each parcellation included for each subregion. The sagittal brain slice is shown at Y = −2.
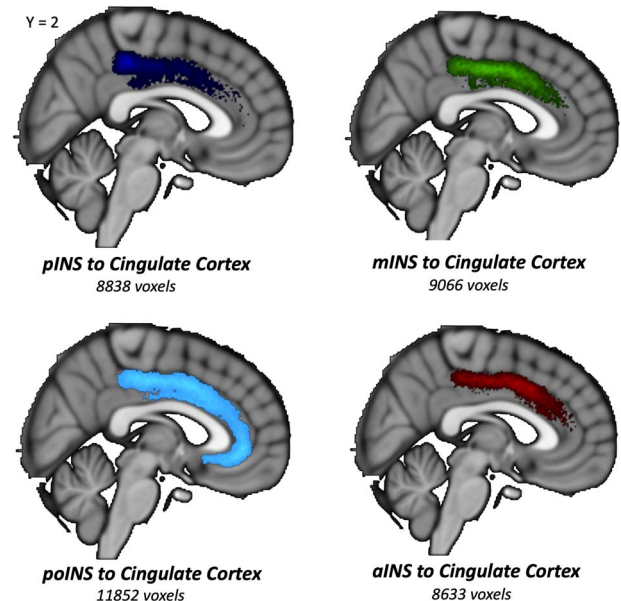

Fig. 5. Right cingulate SC-based parcellation. Group mask of cingulate cortex parcellation based on maximum connectivity probability to insula subregions. Masks thresholded at 25% after creation of mask. Total voxel count of each parcellation included for each subregion. The sagittal brain slice is shown at Y = 2.

sex was also tested, finding significant differences in poINS-pMCC (mean differences = −0.0832; $P = 0.0066$) and poINS-rACC (mean difference = −0.0874; $P = 0.0287$) connectivities in males compared to females. Every insula-cingulate dyad shows significant FC, apart from the rACC's connection to the aINS, mINS, and pINS. Of the insula subregions, the poINS has significant correlations in activity to the aMCC, pMCC, and rACC ($P < 0.00417$; Fig. 6), with a slightly stronger FC to the aMCC. The aINS shows a significant FC to both the aMCC and pMCC ($P < 0.00417$; Fig. 6), with a stronger connection to the aMCC. The mINS and pINS show the same pattern with a significant FC to the aMCC and pMCC ($P < 0.00417$; Fig. 6), again with a stronger connection to the aMCC. Overall, the aINS has the strongest FC to the aMCC, the pINS with the pMCC, and the poINS with the pMCC (Fig. 6).

Right hemisphere

Right FC between each insula-cingulate connectivity is presented in Fig. 6. The effect of age was tested, finding significant differences in the poINS-pMCC ($\rho = 0.0005$; $P = 0.0056$) connectivity. Additionally, the effect of sex was tested, finding no significant effect. Similar to the left hemisphere, every insula-cingulate connection shows significant FC, except for the rACC's connection to the aINS, mINS, and pINS. The poINS has significant correlations in activity to the aMCC, pMCC, and rACC ($P < 0.00417$; Fig. 6), with the strongest FC to the aMCC. The aINS, mINS, and pINS show significant FC to both the aMCC and pMCC ($P < 0.00417$; Fig. 6), with the strongest connections to the aMCC. The aINS shows the
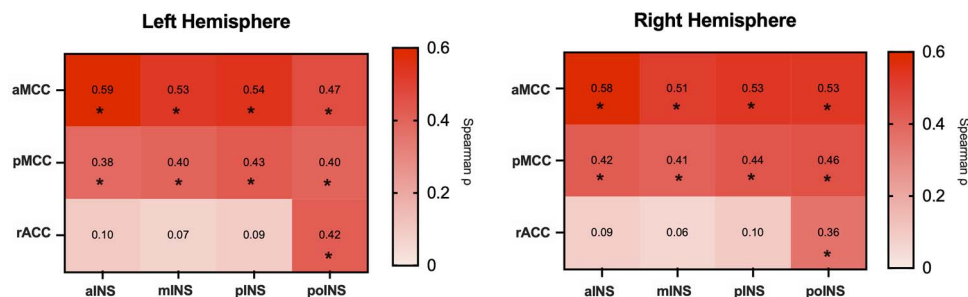
Fig. 6. FC of left and right hemisphere. FC matrix between insula and cingulate subregions, for the left and right hemisphere. Spearman ρ values presented. Significance set at a Bonferroni corrected P < 0.00417.

strongest FC to the aMCC, while the poINS has the strongest FC to both the pMCC and rACC (Fig. 6).

Discussion

In the present study, we aimed to determine the SC and FC between two of the most activated brain regions across all domains of neuroimaging, the insula, and cingulate cortex, and their potential connections within heterogenous networks. Our results highlight significant connectivity differences between insula subregions and the cingulate, as well as significant differences in connectivity strengths within each region.

Many of the models explaining the interaction between the posterior and anterior regions of the insula remains relatively hypothetical. Simply, the aINS responds exclusively to behaviorally salient stimuli, while the pINS responds to interoceptive signals (Frot et al. 2022). With this, we propose that the dense connectivity between the aINS and the aMCC/pMCC are related to their role as key nodes of the SN, as shown previously (Sridharan et al. 2008; Menon and Uddin 2010; Uddin 2015), and function to adjust attention to behaviorally relevant stimuli. We further propose that the strong connection between the pINS and mINS with the pMCC may play a role in interoception. For example, regarding crosstalk in intensity encoding of nociceptive and thermosensory perception (Erpelding et al. 2012; Vogt 2016). Finally, the strong SC of the poINS to all subregions of the cingulate suggests the poINS region may function to relay information from insular subregions to the cingulate, or perhaps other cortical regions.

The SN, involved in the processing of and orienting to salient stimuli, has been the focus of many studies (Seeley et al. 2007; Menon and Uddin 2010; Uddin 2015). Early studies by Downar et al. (2000, 2002, 2003) identified several regions, specifically the aINS and the mid-cingulate cortex (MCC), in the task-independent detection of salient changes in the environment. The aINS is thought to accumulate and process sensory information in decision-making, which then triggers the aMCC to select the appropriate behavioral response (Lamichhane and Dhamala 2015). More recent studies have identified a set of key nodes, including the aINS, aMCC, dorsomedial thalamus, hypothalamus, sublenticular extended amygdala, substantia nigra, periaqueductal gray, and temporal lobe (Seeley et al. 2007). The SN is an important network in integration of interoceptive and visceromotor stimuli, as well as visceroautonomic stimuli, to respond to salient stimuli and guide behavior (Uddin 2015). Abnormalities in SN functioning, specifically between the aINS and aMCC, have been tied to anxiety (DeSerisy et al. 2020), Schizophrenia (SCZ) (White et al. 2010; Spreng et al. 2019), and cognitive impairment [e.g. Alzheimer's Disorder (AD)] (Song et al. 2021), indicating a strong link to cognition.

Our findings focus on the connections of the aINS with cingulate subregions that can be resolved with ultra-high field MRI. The strongest FC of the aINS was with the aMCC in both the right and left hemispheres, consistent with previous studies (Seeley et al. 2007; Taylor et al. 2009; Menon and Uddin 2010; Wiech et al. 2014; Uddin 2015). Additionally, there was also a significant FC with the pMCC, indicating the aINS connection with the MCC in SN functioning may not be limited to the aMCC, rather it encapsulates the MCC. It has been posited that these signals from the aINS project to the anterior-cingulate cortex (ACC), which includes the rACC and aMCC, and influence motor activity (Seeley et al. 2011), given the significant corticospinal tracts originating from this region (Dum et al. 2019). Alternatively, (Menon 2015) hypothesized that the pMCC plays a role in motor response to salient stimuli through the connection with the aMCC. Our SC analysis shows a preferential SC of the aINS to the pMCC, rather than the aMCC, especially within the left hemisphere. Additionally, our connectivity-based parcellation of the cingulate and insula showed that aMCC SC to the insula was largely to the aINS, while the pMCC connects to both the pINS/mINS as well as the aINS, especially within the left hemisphere. Correspondingly, aINS connections were largely to the aMCC and pMCC. This suggests that the aINS connections may first reach the pMCC before further projecting to the aMCC, and onwards to the rACC, in a sort of processing gradient.

Previous studies have found that ascending visceroautonomic and interoceptive signals were first integrated in the aINS before projecting to other cortical regions, suggesting that the insula plays a key role in the guidance of subjective decision-making (Seeley et al. 2011; Uddin 2015). Further, the aINS is preferentially activated in response to arousing socioaffective stimuli, indicating a strong affective-motivational functioning within the aINS (Han et al. 2018). A recent study found that the pINS connection with the SN is positively correlated with interoceptive awareness (Chong et al. 2017). The pINS is a known insular hub that receives interoceptive and visceroautonomic sensory input, which then projects to the aINS (Craig 2002; Critchley 2004; Menon 2015). Though pINS–aINS connection was not directly studied, we did find a significant FC between the pINS and the aINS, but a weaker SC. Paired with findings of cingulate connection with spinal and subcortical ocular motor areas (Fries 1984), it is posited that the pINS revives interoceptive and visceroautonomic stimuli projecting forward to aINS, where it integrates multimodal sensory information and transmits this information to the aMCC for a motor response to the sensory input (Menon and Uddin 2010).

The exact path of the multimodal sensory information to the aINS remains inconclusive, although it is believed that the insula exhibits gradient processing. Due to the cytoarchitectural heterogeneity and differing spinothalamic connections of insular subregions, it is thought that there is hierarchical processing of sensory inputs: lower processing occurs in the posterior regions of

the insula before transitioning to mid and anterior portions, where the cognitive-motivational processing of salient stimuli occurs (Craig 2002; Veréb et al. 2021).

Taken together, the evidence suggests that both the aINS and pINS play important roles in the processing of salient information involving crosstalk with the aMCC and pMCC. As previously proposed by Taylor et al. (2009), there appear to be two systems within the insula that respond to salient stimuli: a more general salience response to interoceptive information, including thermosensory and nociceptive information, involving the pINS and the pMCC/aMCC; and a second system having key functions within the larger SN that responds to emotionally and behaviorally relevant stimuli, involving the aINS and aMCC/pMCC. This first system involving the pINS functions to first filter interoceptive information regarding the physiological state of the entire body before relaying the information beyond to the aINS and the SN for socioaffective analysis (Craig 2002; Critchley 2004).

These findings stem from the differences in functioning of the pINS and the aINS. The aINS has been shown to be activated in emotion (Büchel et al. 1998; Phillips et al. 1998), empathy (Singer 2006), empathy relating to pain (Fallon et al. 2020; Zhou et al. 2020), emotional components of pain (Peyron et al. 2000), and complex emotional states along with the aMCC (Immordino-Yang et al. 2009). The pINS, on the other hand, is involved in the perception of bodily sensations, processing of interoceptive information, awareness of internal states (Uddin et al. 2017), as well as the response to pain intensity with the pMCC (Oertel et al. 2012; Geuter et al. 2017; Malejko et al. 2018).

The SC of the SN in the literature, with focus on the aMCC and aINS, is relatively inconsistent. FC is not directly correlated with white matter connectivity, a notion confirmed by our results: the SC of the aINS is significantly stronger to the pMCC, especially in the left hemisphere, and more weakly connected with the aMCC. These findings are inconsistent with the FC findings of the study but may indicate a third cortical region that projects white matter fibers from the aINS to the aMCC, perhaps via the pMCC. Animal studies have observed some connection between the aINS and aMCC (Qadir et al. 2018), as both regions are hypothesized to have similar ascending spinal pathways linked to interoception (Craig 2002, 2003). Previous tractography studies also report inconsistent results regarding the strength of white matter connections between these regions (Beckmann et al. 2009; van den Heuvel et al. 2009).

In our rs-fMRI analysis, the aINS exhibited nonsignificant FC, and a weak SC, with the rACC. Previous studies have shown that the rACC acts as a key hub of the DMN and the strength of white matter connectivity with the aINS has been observed as a predictor of depression improvement (Whitton et al. 2019). The SN acts as a hub shifting activity from the DMN to the CEN, in response to salient stimuli (Sridharan et al. 2008; Menon and Uddin 2010; Manuello et al. 2018; Varjacic et al. 2018; Li et al. 2022). Therefore, it would be assumed that the aINS and rACC would have a strong FC, as they are consistently co-activated in the functioning of SN shifting of the DMN. Dysfunction in DMN and SN functional coupling has been shown in Parkinson's disease (Putcha et al. 2016), indicating the key role the SN has in cognition. Additionally, both SC and FC alterations have been shown to be implicated in SCZ and Major Depressive Disorder (Shao et al. 2018). Although it is possible the lack of FC between the aINS and rACC, observed in this study, could be due to a lack of demand of the SN during resting-state imaging, previous studies have still implicated changes in the regions during rs-fMRI imaging

(Shao et al. 2018). Therefore, another possible explanation for the lack of SC and FC seen between these two regions is that the crosstalk between the SN and DMN may not be isolated to the aINS-rACC connection and could instead occur through other regions of each network. Alternatively, the significant SC and FC between the poINS (sometimes referred to as the ventral aINS) and the rACC, as well as the strong preferential connection of the rACC to the poINS region in the SC-based parcellation of the insula, could indicate that the poINS is a region of the SN directly responsible for the shift between the DMN and CEN. Previously the dorsal aINS was hypothesized to have this function (Uddin 2016).

Beyond the classical SN, (Taylor et al. 2009) proposed that the entire insula's connectivity to specifically the pMCC is involved in general salience and response selection. The finding of a general strong connection between insular subregions and the pMCC was only seen within the SC findings and were not replicated within FC. In contrast to their findings, we instead found a general bilateral FC preference of insula subregions to the aMCC, while finding a SC preference to the pMCC. This could indicate that perhaps this general salience functioning involving the entire insula may in fact be the relaying of salient information to the general SN from the pINS to the aINS, through to the aMCC, perhaps being relayed through the pMCC. Further research is needed to determine the presence of a distinct general salience versus emotional SN, rather than the relaying of general interoceptive stimuli from the pINS, and perhaps the pMCC, to the aINS and aMCC for subjective analysis.

Insula and cingulate connectivity in nociception and thermosensation

Studies have determined that the insula is involved in all dimensions of pain, including pain affect and intensity (Treede et al. 1999; Hofbauer et al. 2001). Our study found significant FC between the pINS, aINS, and aMCC, consistent with the hypothesis of a gradient transition from sensory-discriminative of pain, in the pINS, to affective-motivational dimensions, in the aINS, before transitioning beyond to the aMCC (Starr et al. 2009; Veréb et al. 2021).

Some argue that the primary pain, or at least initial pain, and thermosensory cortex may be processed in the pINS (Brooks et al. 2002; Ostrowsky et al. 2002; Friebel et al. 2011; Stephani et al. 2011; Lerman et al. 2019), while a slightly later affective response occurs within the aINS (Garcia-Larrea and Bastuji 2018). Additionally, nociceptive neurons have been identified, both in vivo (Hutchison et al. 1999) and ex vivo (Dum et al. 2009), within the pMCC, and have been hypothesized to play a role in the early processing of pain intensity alongside the pINS (Büchel et al. 2002; Vogt 2016; Geuter et al. 2017), although its role is less clear. Our findings show a strong SC between the pINS and pMCC, particularly within the right hemisphere, similar to what has been shown in lower resolution studies (Wiech et al. 2014). This connection between the pMCC and pINS could indicate a key structural substrate for noxious stimuli, although further research is needed.

poINS as a relay node

We also found significant SC from the poINS to all cingulate subregions, which was further confirmed using connectivity-based parcellation of the cingulate cortex. The homogeneity of poINS SC to all cingulate subregions indicates a potential relay node in the ventral aINS. Interestingly, any significant difference in FC when comparing age or sex was isolated to poINS connectivities with

the pMCC and rACC in the left hemisphere, but only significant differences in FC comparing ages were seen in the poINS connection with the pMCC in the right hemisphere.

Research on the poINS is limited, with most insula studies focusing on the pINS or aINS. Studies typically refer to the pole as the ventral aINS (Uddin 2015; Klugah et al. 2022), while other insular parcellation studies classify it based on its anatomical name: the transverse insular gyrus (Richardson and Fridriksson 2016). A study by Ghaziri et al. (2015) analyzed the SC of 19 bilateral insular subregions and found that within the cingulate, the poINS was only connected with the anterior cingulate. Another study found that the poINS has the strongest SC with the rACC (Deen et al. 2011). Although our DWI findings did not show a slight preferential connection to the pMCC, our connectivity-based parcellation of the insula showed that rACC connection is clustered to the poINS, supporting these previous lower resolution findings. These findings could suggest insular tracts first enter the cingulate at the pMCC before traveling anteriorly to the aMCC and rACC. A more recent high-resolution study found that the left poINS has strong connectivity with the frontoparietal network and was related to working memory, while in the right hemisphere this connectivity was shown to be involved in pain (Klugah et al. 2022). Working memory increases have been shown to increase SN connectivity with the DMN and CEN (Liang et al. 2016). Our FC findings along with the findings of Klugah et al. (2022) indicate that the poINS may have connections with the SN. In the direct scope of our study, we propose, consistent with Veréb et al. (2021), that sensory stimuli enter the pINS, transition to the aINS, and finally transverse through the poINS, acting as a relay node, toward the cingulate.

Limitations

The directionality of the identified connections remains unknown and is a limitation of the study. No conclusions regarding the causal connectivity between these regions can be discerned. Direct FC and SC between different insula subregions with each other cannot be discerned. Further research on the causal connection between insula and cingulate subregions in SN, nociceptive processing, and pain-related networks, and the poINS relay node is needed.

Conclusion

Our study used ultra-high field DWI and rs-fMRI data to highlight the key pathways between the insula and cingulate cortex. We found corroborative evidence of an aINS and aMCC connection consistent with that proposed in the SN. The relatively weaker SC between these two regions could indicate a third region between the direct communication of the aINS and aMCC. We found a strong SC and FC between the pINS and pMCC, which could have a potential role in nociceptive processing, specifically pain intensity. However, further research is needed using both direct pain stimulation and the whole brain analysis to identify other regions that respond to noxious stimuli. Lastly, we identified the poINS as a potential relay node for structural white matter tracts to the cingulate, although further research is required to confirm this hypothesis.

Supplementary material

Supplementary material can be found at *Cerebral Cortex* online.

Author contributions

Matthew A. Cormie (Data curation, Formal analysis, Investigation, Methodology, Writing—original draft, Writing—review & editing), Batu Kaya (Methodology, Writing—review & editing), Georgia E. Hadjis (Writing—review & editing), Pedram Mouseli (Data curation, Software, Writing—review & editing), and Massieh Moayedi (Conceptualization, Methodology, Project administration, Supervision, Writing—review & editing).

Data availability

Data are publicly available through the Human Connectome Project (https://www.humanconnectome.org/study/hcp-young-adult).

References

Andersson JLR, Sotiropoulos SN. Non-parametric representation and prediction of single- and multi-shell diffusion-weighted mri data using gaussian processes. *NeuroImage*. 2015:122:166–176.

Andersson JL, Skare S, Ashburner J. How to correct susceptibility distortions in spin-echo echo-planar images: application to diffusion tensor imaging. *NeuroImage*. 2003:20(2):870–888.

Augustine JR. Circuitry and functional aspects of the insular lobe in primates including humans. *Brain Res Rev*. 1996:22(3): 229–244.

Beckmann M, Johansen-Berg H, Rushworth MF. Connectivity-based parcellation of human cingulate cortex and its relation to functional specialization. *J Neurosci*. 2009:29(4):1175–1190.

Behrens TE, Woolrich MW, Jenkinson M, Johansen-Berg H, Nunes RG, Clare S, Matthews PM, Brady JM, Smith SM. Characterization and propagation of uncertainty in diffusion-weighted mr imaging. *Magn Reson Med*. 2003:50(5):1077–1088.

Behrens TEJ, Berg HJ, Jbabdi S, Rushworth MFS, Woolrich MW. Probabilistic diffusion tractography with multiple fibre orientations: what can we gain? *NeuroImage*. 2007:34(1):144–155.

Brooks JCW, Nurmikko TJ, Bimson WE, Singh KD, Roberts N. Fmri of thermal pain: effects of stimulus laterality and attention. *NeuroImage*. 2002:15(2):293–301.

Brooks JCW, Zambreanu L, Godinez A, Craig AD, Tracey I. Somatotopic organisation of the human insula to painful heat studied with high resolution functional imaging. *NeuroImage*. 2005:27(1): 201–209.

Büchel C, Morris J, Dolan RJ, Friston KJ. Brain systems mediating aversive conditioning: an event-related fmri study. *Neuron*. 1998:20(5):947–957.

Büchel C, Bornhovd K, Quante M, Glauche V, Bromm B, Weiller C. Dissociable neural responses related to pain intensity, stimulus intensity, and stimulus awareness within the anterior cingulate cortex: a parametric single-trial laser functional magnetic resonance imaging study. *J Neurosci*. 2002:22(3):970–976.

Caruyer E, Lenglet C, Sapiro G, Deriche R. Design of multishell sampling schemes with uniform coverage in diffusion mri. *Magn Reson Med*. 2013:69(6):1534–1540.

Chong JSX, Ng GJP, Lee SC, Zhou J. Salience network connectivity in the insula is associated with individual differences in interoceptive accuracy. *Brain Struct Funct*. 2017:222(4):1635–1644.

Cloutman LL, Binney RJ, Drakesmith M, Parker GJM, Lambon Ralph MA. The variation of function across the human insula mirrors its patterns of structural connectivity: evidence from in vivo probabilistic tractography. *NeuroImage*. 2012:59(4):3514–3521.

Craig AD. How do you feel? Interoception: the sense of the physiological condition of the body. *Nat Rev Neurosci*. 2002:3(8):655–666.

Craig AD. Interoception: the sense of the physiological condition of the body. *Curr Opin Neurobiol*. 2003:13(4):500–505.

Craig AD. How do you feel–now? The anterior insula and human awareness. *Nat Rev Neurosci*. 2009:10(1):59–70.

Critchley HD. The human cortex responds to an interoceptive challenge. *Proc Natl Acad Sci USA*. 2004:101(17):6333–6334.

Dale AM, Fischl B, Sereno MI. Cortical surface-based analysis. I. Segmentation and surface reconstruction. *NeuroImage*. 1999:9(2):179–194.

Deen B, Pitskel NB, Pelphrey KA. Three systems of insular functional connectivity identified with cluster analysis. *Cerebral Cortex (New York, NY: 1991)*. 2011:21(7):1498–1506.

Descoteaux M, Deriche R, Knösche TR, Anwander A. Deterministic and probabilistic tractography based on complex fibre orientation distributions. *IEEE Trans Med Imaging*. 2009:28(2):269–286.

DeSerisy M, Musial A, Comer JS, Roy AK. Functional connectivity of the anterior insula associated with intolerance of uncertainty in youth. *Cognitive Affective Behav Neurosci*. 2020:20(3):493–502.

Desikan RS, Ségonne F, Fischl B, Quinn BT, Dickerson BC, Blacker D, Buckner RL, Dale AM, Maguire RP, Hyman BT, et al. An automated labeling system for subdividing the human cerebral cortex on mri scans into gyral based regions of interest. *NeuroImage*. 2006:31(3):968–980.

Downar J, Crawley AP, Mikulis DJ, Davis KD. A multimodal cortical network for the detection of changes in the sensory environment. *Nat Neurosci*. 2000:3(3):277–283.

Downar J, Crawley AP, Mikulis DJ, Davis KD. A cortical network sensitive to stimulus salience in a neutral behavioral context across multiple sensory modalities. *J Neurophysiol*. 2002:87(1):615–620.

Downar J, Mikulis DJ, Davis KD. Neural correlates of the prolonged salience of painful stimulation. *NeuroImage*. 2003:20(3):1540–1551.

Dum RP, Levinthal DJ, Strick PL. The spinothalamic system targets motor and sensory areas in the cerebral cortex of monkeys. *J Neurosci*. 2009:29(45):14223–14235.

Dum RP, Levinthal DJ, Strick PL. The mind-body problem: circuits that link the cerebral cortex to the adrenal medulla. *Proc Natl Acad Sci USA*. 2019:116(52):26321–26328.

Dyvorne H, O'Halloran R, Balchandani P. Ultrahigh field single-refocused diffusion weighted imaging using a matched-phase adiabatic spin echo (mase). *Magn Reson Med*. 2016:75(5):1949–1957.

Eisenberger NI, Lieberman MD, Williams KD. Does rejection hurt? An fmri study of social exclusion. *Science (New York, NY)*. 2003:302(5643):290–292.

Erpelding N, Moayedi M, Davis KD. Cortical thickness correlates of pain and temperature sensitivity. *Pain*. 2012:153(8):1602–1609.

Fallon N, Roberts C, Stancak A. Shared and distinct functional networks for empathy and pain processing: a systematic review and meta-analysis of fmri studies. *Soc Cogn Affect Neurosci*. 2020:15(7):709–723.

Feinberg DA, Moeller S, Smith SM, Auerbach E, Ramanna S, Gunther M, Glasser MF, Miller KL, Ugurbil K, Yacoub E. Multiplexed echo planar imaging for sub-second whole brain fmri and fast diffusion imaging. *PLoS One*. 2010:5(12):e15710.

Friebel U, Eickhoff SB, Lotze M. Coordinate-based meta-analysis of experimentally induced and chronic persistent neuropathic pain. *NeuroImage*. 2011:58(4):1070–1080.

Fries W. Cortical projections to the superior colliculus in the macaque monkey: a retrograde study using horseradish peroxidase. *J Comp Neurol*. 1984:230(1):55–76.

Frot M, Mauguière F, Garcia-Larrea L. Insular dichotomy in the implicit detection of emotions in human faces. *Cereb Cortex*. 2022:32(19):4215–4228.

Garcia-Larrea L, Bastuji H. Pain and consciousness. *Prog Neuro-Psychopharmacol Biol Psychiatry*. 2018:87(Pt B):193–199.

Geuter S, Boll S, Eippert F, Büchel C. Functional dissociation of stimulus intensity encoding and predictive coding of pain in the insula. *elife*. 2017:6:e24770.

Ghaziri J, Tucholka A, Girard G, Houde J-C, Boucher O, Gilbert G, Descoteaux M, Lippé S, Rainville P, Nguyen DK. The corticocortical structural connectivity of the human insula. *Cereb Cortex*. 2015:27(2):1216–1228.

Glasser MF, Sotiropoulos SN, Wilson JA, Coalson TS, Fischl B, Andersson JL, Xu J, Jbabdi S, Webster M, Polimeni JR, et al. The minimal preprocessing pipelines for the human connectome project. *NeuroImage*. 2013:80:105–124.

Griffanti L, Salimi-Khorshidi G, Beckmann CF, Auerbach EJ, Douaud G, Sexton CE, Zsoldos E, Ebmeier KP, Filippini N, Mackay CE, et al. Ica-based artefact removal and accelerated fmri acquisition for improved resting state network imaging. *NeuroImage*. 2014:95:232–247.

Han SW, Eaton HP, Marois R. Functional fractionation of the cingulo-opercular network: alerting insula and updating cingulate. *Cereb Cortex*. 2018:29(6):2624–2638.

Hettmansperger TP. Nonparametric rank tests. In: Lovric M, editors. *International encyclopedia of statistical science*. Berlin, Heidelberg: Springer Berlin Heidelberg; 2011. pp. 970–972

van den Heuvel MP, Mandl RC, Kahn RS, Hulshoff Pol HE. Functionally linked resting-state networks reflect the underlying structural connectivity architecture of the human brain. *Hum Brain Mapp*. 2009:30(10):3127–3141.

Hofbauer RK, Rainville P, Duncan GH, Bushnell MC. Cortical representation of the sensory dimension of pain. *J Neurophysiol*. 2001:86(1):402–411.

Hutchison WD, Davis KD, Lozano AM, Tasker RR, Dostrovsky JO. Pain-related neurons in the human cingulate cortex. *Nat Neurosci*. 1999:2(5):403–405.

Immordino-Yang MH, McColl A, Damasio H, Damasio A. Neural correlates of admiration and compassion. *Proc Natl Acad Sci USA*. 2009:106(19):8021–8026.

Jbabdi S, Sotiropoulos SN, Savio AM, Graña M, Behrens TE. Model-based analysis of multishell diffusion mr data for tractography: how to get over fitting problems. *Magn Reson Med*. 2012:68(6):1846–1855.

Jenkinson M, Smith S. A global optimisation method for robust affine registration of brain images. *Med Image Anal*. 2001:5(2):143–156.

Jenkinson M, Bannister P, Brady M, Smith S. Improved optimization for the robust and accurate linear registration and motion correction of brain images. *NeuroImage*. 2002:17(2):825–841.

Jenkinson M, Beckmann CF, Behrens TE, Woolrich MW, Smith SM. FSL. *NeuroImage*. 2012:62(2):782–790.

Jeurissen B, Descoteaux M, Mori S, Leemans A. Diffusion mri fiber tractography of the brain. *NMR Biomed*. 2019:32(4):e3785.

Johansen-Berg H, Behrens TEJ, Robson MD, Drobnjak I, Rushworth MFS, Brady JM, Smith SM, Higham DJ, Matthews PM. Changes in connectivity profiles define functionally distinct regions in human medial frontal cortex. *Proc Natl Acad Sci*. 2004:101(36): 13335–13340.

Jovicich J, Czanner S, Greve D, Haley E, van der Kouwe A, Gollub R, Kennedy D, Schmitt F, Brown G, Macfall J, et al. Reliability in multi-site structural mri studies: effects of gradient non-linearity correction on phantom and human data. *NeuroImage*. 2006:30(2): 436–443.

Kerby DS. The simple difference formula: an approach to teaching nonparametric correlation. *Comprehensive Psychol*. 2014:3: 11.IT.13.11.

Klugah-Brown B, Wang P, Jiang Y, Becker B, Hu P, Uddin LQ, Biswal B. Structural–functional connectivity mapping of the insular cortex: a combined data-driven and meta-analytic topic mapping. *Cerebral Cortex*. 2023:33(5):1726–1738.

Kurlowicz L, Wallace M. The mini-mental state examination (mmse). *J Gerontol Nurs*. 1999:25(5):8–9.

Kurth F, Zilles K, Fox PT, Laird AR, Eickhoff SB. A link between the systems: functional differentiation and integration within the human insula revealed by meta-analysis. *Brain Struct Funct*. 2010:214(5–6):519–534.

Lamichhane B, Dhamala M. The salience network and its functional architecture in a perceptual decision: an effective connectivity study. *Brain Connectivity*. 2015:5(6):362–370.

Lerman I, Davis B, Huang M, Huang C, Sorkin L, Proudfoot J, Zhong E, Kimball D, Rao R, Simon B, et al. Noninvasive vagus nerve stimulation alters neural response and physiological autonomic tone to noxious thermal challenge. *PLoS One*. 2019:14(2):e0201212.

Li H, Goldin P, Siegle GJ. 1.08 - neuroscience for clinicians: Translational clinical neuroscience to inspire clinical practice and research. In: Asmundson GJG, editors. *Comprehensive clinical psychology (second edition)*. Oxford: Elsevier; 2022. pp. 145–167

Liang X, Zou Q, He Y, Yang Y. Topologically reorganized connectivity architecture of default-mode, executive-control, and salience networks across working memory task loads. *Cerebral Cortex (New York, NY: 1991)*. 2016:26(4):1501–1511.

Malejko K, Neff D, Brown RC, Plener PL, Bonenberger M, Abler B, Grön G, Graf H. Somatosensory stimulus intensity encoding in borderline personality disorder. *Front Psychol*. 2018:9:1853.

Manuello J, Nani A, Cauda F. Attention, salience, and self-awareness: The role of insula in meditation. In: Turgut M, Yurttaş C, Tubbs RS, editors. *Island of reil (insula) in the human brain: anatomical, functional, clinical and surgical aspects*. Cham: Springer International Publishing; 2018. pp. 213–221

Menon V. Salience network. In: Toga AW, editors. *Brain mapping*. Waltham: Academic Press; 2015. pp. 597–611

Menon V, Uddin LQ. Saliency, switching, attention and control: a network model of insula function. *Brain Struct Funct*. 2010:214 (5–6):655–667.

Mesulam MM, Mufson EJ. Insula of the old world monkey. I. Architectonics in the insulo-orbito-temporal component of the paralimbic brain. *J Comp Neurol*. 1982a:212(1):1–22.

Mesulam MM, Mufson EJ. Insula of the old world monkey. Iii: Efferent cortical output and comments on function. *J Comp Neurol*. 1982b:212(1):38–52.

Mishra P, Pandey CM, Singh U, Gupta A, Sahu C, Keshri A. Descriptive statistics and normality tests for statistical data. *Ann Card Anaesth*. 2019:22(1):67–72.

Moeller S, Yacoub E, Olman CA, Auerbach E, Strupp J, Harel N, Uğurbil K. Multiband multislice ge-epi at 7 tesla, with 16-fold acceleration using partial parallel imaging with application to high spatial and temporal whole-brain fmri. *Magn Reson Med*. 2010:63(5):1144–1153.

Mufson EJ, Mesulam MM. Insula of the old world monkey. Ii: Afferent cortical input and comments on the claustrum. *J Comp Neurol*. 1982:212(1):23–37.

Mukherjee P, Hess CP, Xu D, Han ET, Kelley DA, Vigneron DB. Development and initial evaluation of 7-t q-ball imaging of the human brain. *Magn Reson Imaging*. 2008:26(2):171–180.

Oertel BG, Preibisch C, Martin T, Walter C, Gamer M, Deichmann R, Lötsch J. Separating brain processing of pain from that of stimulus intensity. *Hum Brain Mapp*. 2012:33(4):883–894.

Ostrowsky K, Magnin M, Ryvlin P, Isnard J, Guenot M, Mauguière F. Representation of pain and somatic sensation in the human insula: a study of responses to direct electrical cortical stimulation. *Cerebral Cortex (New York, NY: 1991)*. 2002:12(4):376–385.

Peyron R, Laurent B, García-Larrea L. Functional imaging of brain responses to pain. A review and meta-analysis (2000). *Neurophysiol Clin = Clin Neurophysiol*. 2000:30(5):263–288.

Phillips ML, Young AW, Scott S, Calder AJ, Andrew C, Giampietro V, Williams SCR, Bullmore ET, Brammer M, Gray JA. Neural responses to facial and vocal expressions of fear and disgust. *Proc R Soc Lond Series B Biol Sci*. 1998:265(1408):1809–1817.

Putcha D, Ross RS, Cronin-Golomb A, Janes AC, Stern CE. Salience and default mode network coupling predicts cognition in aging and parkinson's disease. *J Int Neuropsychol Soc*. 2016:22(2):205–215.

Qadir H, Krimmel SR, Mu C, Poulopoulos A, Seminowicz DA, Mathur BN. Structural connectivity of the anterior cingulate cortex, claustrum, and the anterior insula of the mouse. *Front Neuroanat*. 2018:12:100.

Richardson JD, Fridriksson J. Chapter 10 – The insular cortex. In: Hickok G, Small SL, editors. *Neurobiology of language*. San Diego: Academic Press; 2016. pp. 115–127

Rolls ET. The cingulate cortex and limbic systems for emotion, action, and memory. *Brain Struct Funct*. 2019:224(9):3001–3018.

Salimi-Khorshidi G, Douaud G, Beckmann CF, Glasser MF, Griffanti L, Smith SM. Automatic denoising of functional mri data: combining independent component analysis and hierarchical fusion of classifiers. *NeuroImage*. 2014:90:449–468.

Seeley WW, Menon V, Schatzberg AF, Keller J, Glover GH, Kenna H, Reiss AL, Greicius MD. Dissociable intrinsic connectivity networks for salience processing and executive control. *J Neurosci*. 2007:27(9):2349–2356.

Seeley WW, Merkle FT, Gaus SE, Craig AD, Allman JM, Hof PR. Distinctive neurons of the anterior cingulate and frontoinsular cortex: a historical perspective. *Cereb Cortex*. 2011:22(2): 245–250.

Setsompop K, Gagoski BA, Polimeni JR, Witzel T, Wedeen VJ, Wald LL. Blipped-controlled aliasing in parallel imaging for simultaneous multislice echo planar imaging with reduced g-factor penalty. *Magn Reson Med*. 2012:67(5):1210–1224.

Shao J, Meng C, Tahmasian M, Brandl F, Yang Q, Luo G, Luo C, Yao D, Gao L, Riedl V, et al. Common and distinct changes of default mode and salience network in schizophrenia and major depression. *Brain Imaging Behav*. 2018:12(6):1708–1719.

Singer T. The neuronal basis and ontogeny of empathy and mind reading: review of literature and implications for future research. *Neurosci Biobehav Rev*. 2006:30(6):855–863.

Singer T, Seymour B, O'Doherty J, Kaube H, Dolan RJ, Frith CD. Empathy for pain involves the affective but not sensory components of pain. *Science (New York, NY)*. 2004:303(5661):1157–1162.

Song Y, Xu W, Chen S, Hu G, Ge H, Xue C, Qi W, Lin X, Chen J. Functional mri-specific alterations in salience network in mild cognitive impairment: an ale meta-analysis. *Front Aging Neurosci*. 2021:13:695210.

Spreng RN, DuPre E, Ji JL, Yang G, Diehl C, Murray JD, Pearlson GD, Anticevic A. Structural covariance reveals alterations in control and salience network integrity in chronic schizophrenia. *Cerebral Cortex (New York, NY: 1991)*. 2019:29(12):5269–5284.

Sridharan D, Levitin DJ, Menon V. A critical role for the right fronto-insular cortex in switching between central-executive and default-mode networks. *Proc Natl Acad Sci USA*. 2008:105(34): 12569–12574.

Starr CJ, Sawaki L, Wittenberg GF, Burdette JH, Oshiro Y, Quevedo AS, Coghill RC. Roles of the insular cortex in the modulation of pain: insights from brain lesions. *J Neurosci*. 2009:29(9):2684–2694.

Stephani C, Fernandez-Baca Vaca G, Maciunas R, Koubeissi M, Lüders HO. Functional neuroanatomy of the insular lobe. *Brain Struct Funct*. 2011:216(2):137–149.

Taylor KS, Seminowicz DA, Davis KD. Two systems of resting state connectivity between the insula and cingulate cortex. *Hum Brain Mapp*. 2009:30(9):2731–2745.

Treede R-D, Kenshalo DR, Gracely RH, Jones AKP. The cortical representation of pain. *Pain*. 1999:79(2):105–11.

Türe U, Yaşargil DCH, Al-Mefty O, Yaşargil MG. Topographic anatomy of the insular region. *J Neurosurg*. 1999:90(4):720–733.

Uddin LQ. Salience processing and insular cortical function and dysfunction. *Nat Rev Neurosci*. 2015:16(1):55–61.

Uddin LQ. *Salience network of the human brain*. Academic Press, Cambridge, MA, 2016.

Uddin LQ, Nomi JS, Hébert-Seropian B, Ghaziri J, Boucher O. Structure and function of the human insula. *J Clin Neurophysiol Off Publ Am Electroencephalographic Soc*. 2017:34(4):300–306.

Van Essen DC, Ugurbil K, Auerbach E, Barch D, Behrens TE, Bucholz R, Chang A, Chen L, Corbetta M, Curtiss SW, et al. The human connectome project: a data acquisition perspective. *NeuroImage*. 2012:62(4):2222–2231.

Van Essen DC, Smith SM, Barch DM, Behrens TEJ, Yacoub E, Ugurbil K. The wu-minn human connectome project: an overview. *NeuroImage*. 2013:80:62–79.

Van Essen DC, Jbabdi S, Sotiropoulos SN, Chen C, Dikranian K, Coalson T, Harwell J, Behrens TEJ, Glasser MF. Chapter 16 - mapping connections in humans and non-human primates: Aspirations and challenges for diffusion imaging. In: Johansen-Berg H, Behrens TEJ, editors. *Diffusion mri*. second ed. San Diego: Academic Press; 2014. pp. 337–358

Varjacic A, Mantini D, Demeyere N, Gillebert C. Neural signatures of trail making test performance: evidence from lesion-mapping and neuroimaging studies. *Neuropsychologia*. 2018:115: 78–87.

Veréb D, Kincses B, Spisák T, Schlitt F, Szabó N, Faragó P, Kocsis K, Bozsik B, Tóth E, Király A, et al. Resting-state functional heterogeneity of the right insula contributes to pain sensitivity. *Sci Rep*. 2021:11(1):22945.

Vogt BA. Pain and emotion interactions in subregions of the cingulate gyrus. *Nat Rev Neurosci*. 2005:6(7):533–544.

Vogt BA. Midcingulate cortex: structure, connections, homologies, functions and diseases. *J Chem Neuroanat*. 2016:74:28–46.

Vogt BA, Berger GR, Derbyshire SW. Structural and functional dichotomy of human midcingulate cortex. *Eur J Neurosci*. 2003:18(11):3134–3144.

White TP, Joseph V, Francis ST, Liddle PF. Aberrant salience network (bilateral insula and anterior cingulate cortex) connectivity during information processing in schizophrenia. *Schizophr Res*. 2010:123(2–3):105–115.

Whitton AE, Webb CA, Dillon DG, Kayser J, Rutherford A, Goer F, Fava M, McGrath P, Weissman M, Parsey R, et al. Pretreatment rostral anterior cingulate cortex connectivity with salience network predicts depression recovery: findings from the embarc randomized clinical trial. *Biol Psychiatry*. 2019:85(10):872–880.

Wiech K, Jbabdi S, Lin CS, Andersson J, Tracey I. Differential structural and resting state connectivity between insular subdivisions and other pain-related brain regions. *Pain*. 2014:155(10): 2047–2055.

Xu J, Moeller S, Strupp J, Auerbach EJ, Chen L, Feinberg DA, Ugurbil K, Yacoub E. Highly accelerated whole brain imaging using aligned-blipped-controlled-aliasing multiband epi. International Society for Magnetic Resonance in medicine 20th annual meeting. 2012.

Zaki J, Wager TD, Singer T, Keysers C, Gazzola V. The anatomy of suffering: understanding the relationship between nociceptive and empathic pain. *Trends Cogn Sci*. 2016:20(4):249–259.

Zhao H, Turel O, Bechara A, He Q. How distinct functional insular subdivisions mediate interacting neurocognitive systems. *Cerebral*. Cortex.bhac169. 2022:33(5):1739–1751.

Zhou F, Li J, Zhao W, Xu L, Zheng X, Fu M, Yao S, Kendrick KM, Wager TD, Becker B. Empathic pain evoked by sensory and emotional-communicative cues share common and process-specific neural representations. *elife*. 2020:9:e56929.